Two-step manufacturing of hundreds of meter-long silicon micrometer-size core optical fibers with less than 0.2 dB/cm background losses

M. Kudinova, G. Bouwmans, O. Vanvincq, R. Habert, S. Plus, R. Bernard, K. Baudelle, A. Cassez, B. Chazallon, M. Marinova, et al.

M. Kudinova, G. Bouwmans, O. Vanvincq, et al.

View Online   **Export Citation**   **CrossMark**

ARTICLES YOU MAY BE INTERESTED IN

Hybrid InP and SiN integration of an octave-spanning frequency comb
APL Photonics **6**, 026102 (2021); https://doi.org/10.1063/5.0035452

Simple method for mid-infrared optical frequency comb generation with dynamic offset frequency tuning
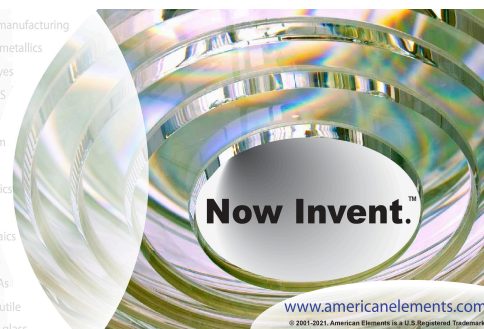APL Photonics **6**, 026103 (2021); https://doi.org/10.1063/5.0038496

Two-dimensional mapping of surface scatterers on an optical fiber core using selective mode launching
APL Photonics **6**, 026105 (2021); https://doi.org/10.1063/5.0036300

Two-step manufacturing of hundreds of meter-long silicon micrometer-size core optical fibers with less than 0.2 dB/cm background losses

M. Kudinova,[1,a)] G. Bouwmans,[1] O. Vanvincq,[1] R. Habert,[1] S. Plus,[1] R. Bernard,[1] K. Baudelle,[1] A. Cassez,[1] B. Chazallon,[1] M. Marinova,[2] N. Nuns,[2] and L. Bigot[1,b)] (iD)

AFFILIATIONS

[1] Univ. Lille, CNRS, UMR 8523–PhLAM–Physique des Lasers Atomes et Molécules, F-59000 Lille, France
[2] Univ. Lille, CNRS, INRA, Centrale Lille, ENSCL, Univ. Artois, FR 2638–IMEC–Institut Michel-Eugène Chevreul, F-59000 Lille, France

[a)] **Now at:** Prysmian Group, Parc des Industries Artois Flandres, 644 boulevard Est, Billy Berclau, 62092 Haisnes Cedex, France.
[b)] **Author to whom correspondence should be addressed:** laurent.bigot@univ-lille.fr

ABSTRACT

This work reports on the fabrication and the characterization of hybrid optical fibers with silicon core and silica cladding. Adopting a two-step manufacturing technique derived from the stack-and-draw method, silicon-core fibers with core dimensions ranging from about 0.8 μm to 3.5 μm have been successively drawn into hundreds of meter-long fibers. A 3.3 μm diameter core fiber has been more extensively characterized and background losses for this as-drawn fiber are less than 0.2 dB/cm between 1250 nm and 1650 nm, with a minimum of 0.12 dB/cm around 1600 nm. The crystalline state of the core and the limited impact of oxygen contamination were confirmed by Raman scattering, x-ray diffraction, HR-STEM, and ToF-SIMS analysis. Transmission peaks associated with specific modal distributions are evidenced under certain injection conditions and their positions are shown to be in good accordance with mode cut-off wavelengths of a step-index silicon-core fiber.

I. INTRODUCTION

Hybrid optical fibers are optical fibers that combine, in the same structure, a glass (generally silica) with a crystal, a metal, a polymer, or a second type of glass. They open access to a wide range of optical properties and functions not accessible to conventional optical fibers.[1] Silicon-core fibers are one type of hybrid fibers that have been intensively studied since 2006 in the case of both hydrogenated amorphous silicon (a-Si:H) and crystalline silicon[2–4] core material. In this work, we will focus our attention on crystalline silicon especially due its transparency in the mid-infrared combined to highly nonlinear properties and the possibilities it offers to implement opto-electrical functions in the optical fiber itself.[3,5] For example, crystalline silicon transmits light on the spectral range between 1.1 μm and 7 μm and hence covers the atmospheric transmission window of strong interest for molecular spectroscopy. Some of the

unique properties of fibers based on such material have been demonstrated in the recent years, but it is admitted that optical losses are still today a limitation to the rise in performances and therefore require specific attention.[5] This is particularly true for the fibers synthesized by the so-called Molten-Core Drawing (MCD) but is also valid for their counterparts obtained from the HPCVD (High Pressure Chemical Vapor Deposition) method. In both cases, as-manufactured/as-drawn fibers present background losses generally much larger than 1 dB/cm at 1.55 μm: about 6 dB/cm for HPCVD-made fibers and 2 dB/cm for MCD-derived fibers.[6] In this last case, this loss level is attributed to the polycrystalline nature of the core material and to oxygen contamination from the silica cladding, which also prevents directly obtaining core diameters smaller than 10 μm, except if oxygen getters are added, which permits the reaching of a core size of 4 μm.[7] Regarding fibers obtained by HPCVD, there is more flexibility on both the core size and the nature of

the as-made core material, generally amorphous and then turned into crystalline via thermal annealing. Such kind of post-processing, based on either thermal annealing or laser treatment, is generally mandatory to improve the quality of the fibers.[8] When applied to HPCVD-made fibers, loss values can be decreased to 0.47 dB/cm –1 dB/cm[9] and even to 0.2 dB/cm–3 dB/cm in the case of MCD-made fibers, which represents today's record in such fibers.[10] However, these techniques have been demonstrated on centimeters-long fibers only, which leads to the conclusion that there is still a lack of process that can make available long (>1 m), small-core (<4 μm), and low-loss (<2 dB/cm) silicon-core fibers.[11] Pieces of such fibers could, without the need of post-processing, be useful for nonlinear applications where a good trade-off between nonlinearity and losses is essential, together with the advantage of the practical commercial use based on an economy of scale. This work aims to put in evidence that silicon core fiber drawing performed on a conventional drawing tower permits the fabrication of easy-to-manipulate silicon-core fibers combining relatively small core dimensions (less than 4 μm in diameter and possibly less than 1 μm) and sub dB/cm loss level. Applying a variant of the MCD, robust pieces of polymer-coated fiber were continuously manufactured over lengths exceeding one hundred of meters, i.e., lengths comparable with those already been reported for fibers manufactured by conventional MCD in the case of silicon[11] or germanium[12] core material. In this last case, the core dimension was significantly larger (15 μm), as well as the temperature mismatch between the glass drawing temperature and the core melting temperature. A panel of structural characterizations has been applied so as to establish the link between the transmission properties of the fiber and the nature of the core material.

II. FIBER MANUFACTURING

As a starting point, a commercially available polycrystalline silicon rod (purity 99.999%, GoodFellow) is inserted into an air/silica stack, similar to what is commonly applied for the fabrication of air/silica Photonic Crystal Fibers (PCFs) by the so-called stack-and-draw process: the method will hence be referred to as the rod-in-stack technique (see the Appendix).

This stack, once sleeved into a jacket tube, has been drawn into a cane under vacuum conditions so as to initiate the collapsing of the structure. Several meter-long and millimeter-size canes were then obtained. One of those canes, free of cracks, has then be sleeved into a second jacket tube and drawn into a fiber under vacuum conditions so as to obtain an all-solid structure. As is done for conventional fibers, a polymer coating is applied on the outer surface of the fiber, which makes it possible to target the continuous drawing of very long fiber samples. Fiber drawing was performed with a remarkable stability of the fiber diameter, which permitted us to get about 160 m of silicon-core fiber in the case of the example discussed in Sec. III. A direct link can be made between the stability of the fiber diameter and the homogeneity of the silicon/silica geometry: our experience reveals that any major modification of the silicon-core geometry because of the different thermal behavior of silicon and silica has a direct signature on the monitoring of the fiber diameter.[13] It is hence deduced from the monitoring of the fiber diameter that the silicon/silica fiber structure is pretty well conserved all along the fiber, which is confirmed by analyzing the transverse fiber structure at several longitudinal positions. This manufacturing process
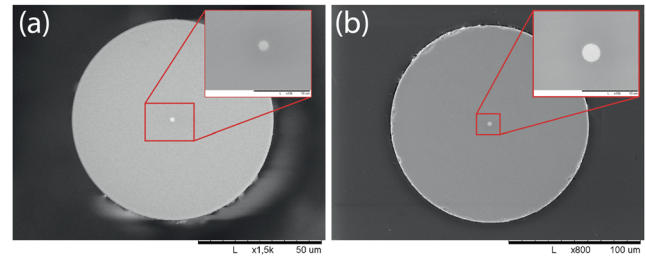

FIG. 1. Examples of SEM images of two silicon-core fibers manufactured by the rod-in-stack method. (a) Fiber with an core diameter of 1.8 μm and a cladding diameter of 81 μm. (b) Fiber with a core diameter of 3.3 μm and a cladding diameter of 146 μm. Inset: zoomed-in view of the core region of these fibers.

has been applied to draw several pieces of fibers with core diameters ranging from 0.8 μm to 3.5 μm by simply changing the draw speed. Scanning Electron Microscope (SEM) images of some of the fibers that have been obtained are presented in Fig. 1. The discussion will now focus on one of these fibers [Fig. 1(b)], whose optical and structural properties have been more extensively studied. The core diameter of this fiber is 3.3 μm and its outer diameter is close to 146 μm. Note that, along the whole fiber span, the mean diameter value is 3.5 μm and its standard deviation is about 430 nm.

III. OPTICAL AND STRUCTURAL CHARACTERIZATIONS

A. Transmission properties

The guiding properties of the 3.3 μm-core fiber have been analyzed using cutback and mode imaging techniques in the Telecom wavelength range. As shown in Fig. 2(a), light transmission is observed on fiber lengths as long as about 1.5 m.

A view of the whole fiber output facet [see Figs. 2(b) and 2(c)] puts in evidence that light is effectively confined in the core of the fiber and that parasitic light from possible cladding modes—expected to be stripped out by the polymer coating—can be considered negligible. This is a first proof of the relatively good transparency of the core material. The fiber being excited using a high-numerical aperture silica fiber (UHNA3, Nufern), one can
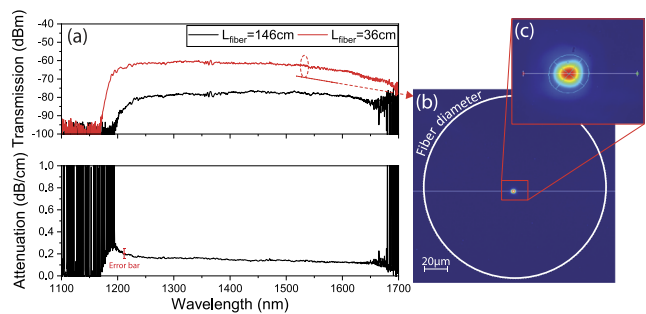

FIG. 2. (a)–(c) Transmission and modal properties of the silicon-core fiber. Left: optical transmission spectra for two different fiber lengths and attenuation curve deduced from those measurements. Right: near field image of the fiber output around 1500 nm wavelength with an imaging system permitting either a view of the whole fiber face or a zoom of the core region (inset).

selectively excite a Gaussian-like mode of the multimode waveguide, as illustrated by Fig. 2(c). The transmission window starts around 1150 nm, which is in accordance with the well-known short-wavelength cutoff of silicon (see Ref. 14). Adopting these injection conditions, optical losses can be deduced from a cutback method and are below 0.2 dB/cm over the transmission window from 1250 nm to 1650 nm, with value approaching 0.12 dB/cm at 1600 nm. This result was confirmed by realizing multiple measurements on different pieces of fiber picked out at different positions along the span. An error bar of 0.05 dB/cm [reported in Fig. 2(a)] has been deduced from these measurements. This result suggests that background losses similar to the best values reported for Silicon-on-Oxide (SOI) waveguides can be achieved for an as-drawn silicon-core fiber, i.e., without the need for an interfacial modifier or for the application of a post-treatment to the fiber, such as a thermal annealing or laser re-crystallization process. Besides the loss value itself, this represents a significant improvement over approaches based on post-processing, which can only achieve low losses over a few centimeters due to constraints with the setup.

The low background losses above-reported are raising the question of the nature of the core material, especially when compared to the state-of-the-art of silicon-core fiber manufacturing. As has been suggested in previous studies, due to possible oxygen contamination from the silica cladding, the MCD seems not adapted to directly obtain small core diameter silicon-core fibers with good optical properties, making the use of oxygen getters and post-processing of the fiber mandatory.[15] Moreover, the background losses reported up to now for as-manufactured fibers, even those possessing a larger core, are typically larger than 2 dB/cm, i.e., at least one order of magnitude larger than the ones reported here. Because the rod-in-stack technique used here presents strong similarities with MCD, one could expect to observe similar optical and structural behaviors for both approaches. Hypotheses can be put forward to try to explain this result, which was confirmed by carrying out multiple characterizations on different fibers and fiber sections made in this way. First, it has to be pointed out that, in addition to a different management of the silicon rod (a rod in an air/silica structure instead of a rod in a tube), different drawing conditions (the equipment itself—for example, the length of the hot zone of the furnace—but also the drawing parameters such as temperature and feeding/drawing speeds) may lead to a different structural behavior (see the Appendix, Table I). Second, it is considered that the use of a two-step process (similar to the approach described in Ref. 16 developed to realize the micrometer-sized silicon-in-silica sphere) permits us to obtain, in a first step, a cane whose core is very large (>300 μm) so that all the diffusion/dissolution processes are limited to the periphery of the core, which has limited impact on the final properties. At this stage, the temperature can be gently lowered after the drop on the silica part to reach the section with silicon under good conditions with a lower draw ratio than during a direct draw. In addition, a significant change in diameter when the silicon arrives is not prohibitive unlike direct fiber drawing or a strong variation in the diameter would be incompatible with the application of a polymer. In the second step, the meter-long cane to be drawn into fiber is long enough to (i) initiate drawing, then (ii) adapt the drawing parameters to reach the suited drawing conditions, and (iii) draw continuously several hundreds of meters of fiber. More precisely, this method enables long fiber lengths to be drawn from a part of the preform that has not

sustained the high temperature and long delay of the drop off, but only both the relatively fast draw speed and low temperature limit the diffusion and dissolution effects that are source of losses. It is now proposed to verify these hypotheses, thanks to different structural studies of the fiber.

B. Structural properties

X-ray Diffraction (XRD) experiments (not shown here) were first performed on a sample of fiber partly etched with hydrofluoric acid and then turned into powder. The diffraction peaks typical of crystalline silicon clearly emerge from the broad signal of the residual amorphous silica cladding material, which indicates the presence of a crystalline phase in the fiber. The crystalline nature of the core is also confirmed by Raman spectroscopy. As illustrated in Fig. 3, a peak around 520 cm^{-1} is put in evidence, which is consistent with a highly crystalline silicon material.[13] The intensity of this peak is strongly reduced when the beam reaches the core/cladding interface. One can note that the position of the peak depends on the position within the core section, which is attributed to tensile stress arising from the difference in the thermal expansion coefficients between silica and silicon.[17]

To go deeper in the investigation of the nature and quality of the core material, Scanning Transmission Electron Microscopy (STEM) has been performed on fiber samples prepared using the Focused Ion Beam (FIB) technique. Thin sections of the sample have been cut both longitudinally and transversely to the fiber axis in order to analyze composition and homogeneity in the fiber volume. At first, in the case of the transverse slice, Selected Area Electron Diffraction (SAED) patterns in the (112) silicon section for different positions in the core section, i.e., in the core itself and at the core/cladding interface, have been studied. High-resolution high-angle annular dark field (HR-HAADF) imaging in STEM mode has also been performed.

This is illustrated in Fig. 4, which brings out a clear structural contrast between the core and the cladding materials: both SAED diffraction patterns and HAADF images demonstrate the amorphous structure of the cladding, whereas in the core and close to the core/cladding interface, the diffraction pattern in the (112) zone
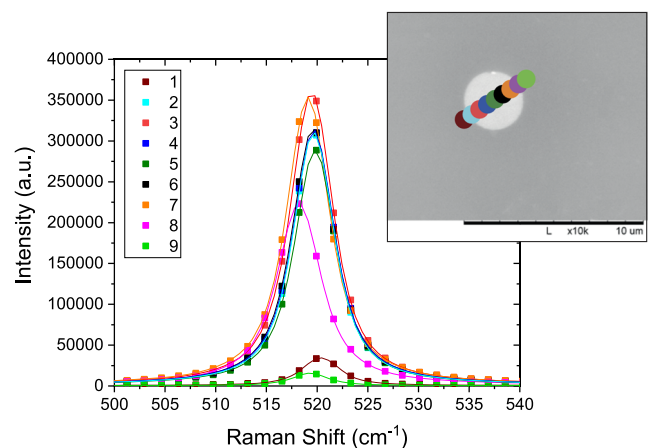

FIG. 3. Raman spectra recorded along a diameter of the 3.3 μm-core fiber. In the inset, the position of the laser spots is superimposed on a SEM image of the fiber.
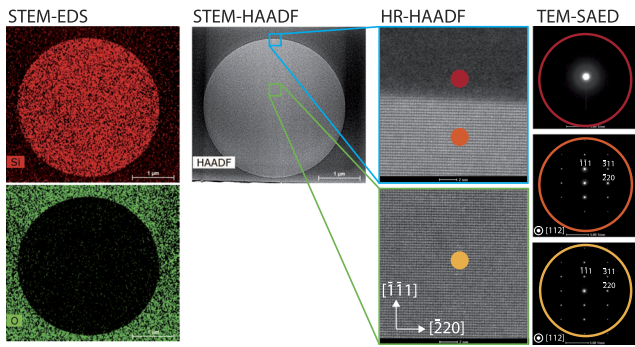
FIG. 4. STEM analysis of the fiber facet. STEM images of the fiber facet together with HR-HAADF and SAED patterns for different positions symbolized by the colored spots (right) and compositional mapping of silicon and oxygen elements (left).

section of silicon is clearly observed. In the HAADF images, the silicon dumbbell spacing in the silicon (112) section of ~80 pm is visible. Compositional mapping (STEM-EDS) of the core region confirms this very good contrast: the circular core is clearly magnified in both silicon and oxygen mapping, with, on one hand, a net difference in silicon concentration between core and cladding. The same analysis performed on the nearly longitudinal sections, within the (101) Si section, permits us to characterize the structural properties along about 28 μm of fiber: the good quality of the core/cladding interface is again confirmed. However, this analysis puts in evidence the presence of three coherent (111) twin interfaces in the middle of the core (see Fig. 5).

The center part of the core consists of two monocrystalline grains in twin crystallographic relation, separated by two twinned nanolamellae having thickness of 11.5 nm and 13.5 nm each (interfaces T1/T2, T2/T1, and T1/T2 in Fig. 5). The twinning appears along the (111) planes as well as the interfaces that separate the lamellae. These (111) interfaces do not present structural distortions. Such a twinning phenomenon is well documented in the literature.[18] These twin boundaries with boundary planes (111) as mirror planes could be created during fiber drawing due to the constraints at the core/cladding interface. However, the structural coherency of these
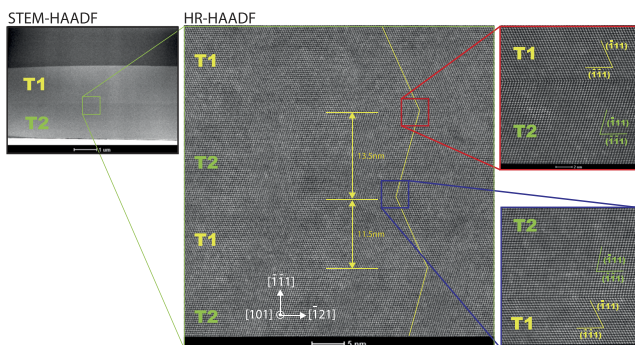
interfaces could explain why the optical quality of the core material is poorly impacted. So as to more accurately investigate the compositional mapping of the core, Time-of-Flight Secondary Ion Mass Spectrometry (ToF-SIMS) has been performed on the longitudinal section of the fiber. This very sensitive surface analytical technique is perfectly adapted to identify the different species and bounding existing in the core and cladding materials. 3D compositional mapping is possible by alternating the compositional analysis and surface sputtering sequences, compositional discrimination being possible thanks to the different times of flight of the different ionic species that are ejected and accelerated toward the detector. In the case of the results presented here, a 19 h run is necessary to travel from one side of the fiber diameter to the other side. By minimizing the delay between sputtering and analysis steps, it is observed that it has been possible to minimize the impact of re-oxidation of the surface—which was not the case for the STEM measurements presented before—a well-known phenomenon in the case of silicon materials. It is hence considered that compositional mappings should, in this case, be very representative of the composition of the sample. As illustrated in Fig. 6, a very good compositional 3D contrast is put in evidence when one chooses to isolate the compositional mapping of the characteristic species of either a pure silica or a pure silicon environment.

Species such as Si_n^- (negative ions formed by n silicon atoms) are typical of a pure silicon matrix and do not exist in SiO_2, which is why we chose them as markers of a pure silicon environment. Inversely, species such as Si^+, SiO^+, or SiO_2^- are typical of a pure silica environment and have been used as markers of a glassy silica material. More information can be found in Ref. 19. The shape of the 28 μm-long piece of fiber is well reconstructed and, when looking deeper in the details, SiO_2^-, SiO_3^-, O^-, or O_2^- species are only detected in the cladding region and not in the core, whereas it is the exact opposite for species such as Si_n^-. Average concentration profiles of an 800 nm thick zone located in the middle of the core region have been reconstructed and are presented in Fig. 7 for Si^-,

FIG. 5. STEM analysis along the fiber. STEM-HAADF images of a longitudinal section of fiber. Right: HR-STEM images of the twin boundary region (middle of the core, green square on the STEM-HAAF image) at different magnifications.

3D Render of SiO$_2^-$　　　3D Render of O$_2^-$

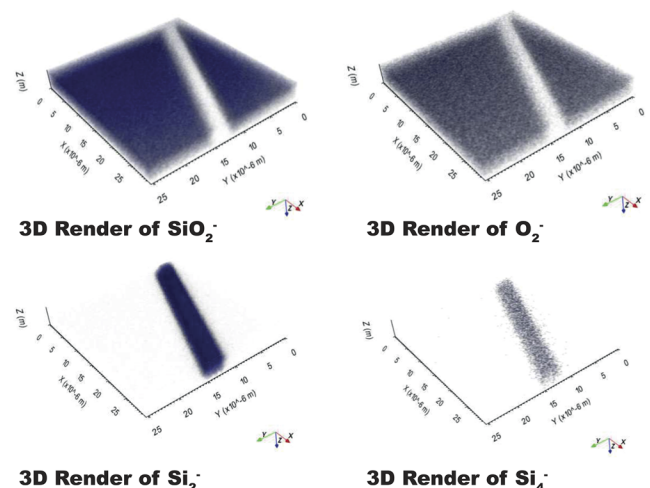3D Render of Si$_2^-$　　　3D Render of Si$_4^-$

FIG. 6. ToF-SIMS analysis of the longitudinal section of the fiber. Top: 3D images of SiO_2^-, O_2^-, Si_2^-, and SiO_4^- species.
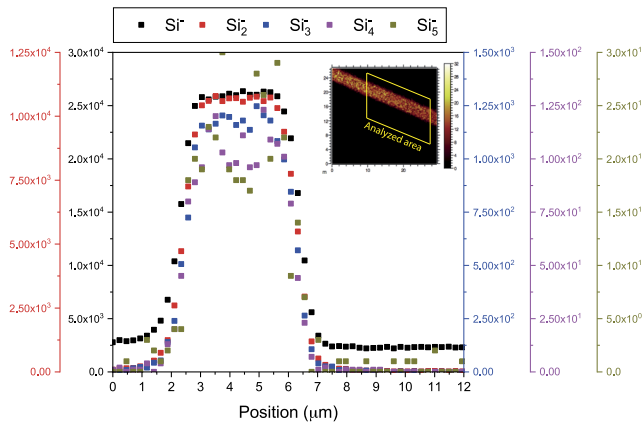
FIG. 7. Semi-quantitative profiles of silicon markers, i.e., Si^-, Si_2^-, Si_3^-, Si_4^-, and Si_5^-.

FIG. 8. Transmission properties under offset injection conditions. Top: optical transmission and intensity distribution at the fiber output of the silicon-core fiber with offset injection (filtered supercontinuum light source). Bottom: modeling of the optical transmission of a fiber with core of 2.9 μm in diameter and with the same offset injection.

Si_2^-, Si_3^-, Si_4^-, and Si_5^-. It is observed that the concentration-related intensity of characteristic species of a pure silicon environment is about three orders of magnitude larger in the core region than in the cladding. The Full Width at Half Maximum (FWHM) of the five curves presented here is about 3.9 μm, which is in accordance with the core diameter measurement first deduced from SEM images. These results suggest that the 3.3 μm silicon-core is well preserved after two drawings (one for the drawing into cane and the second for the drawing into fiber) at 1970 °C and 1900 °C.

All the structural characterizations are converging toward the signature of a pure silicon core, with few impacted by oxygen diffusion and presenting an optical quality comparable to the state of the art of SOI waveguides. So as to attest that light is effectively guided in the silicon core, a supplementary experiment has been carried out so as to probe the modal content of the guided light and compare it to what is theoretically expected for a silicon–silica waveguide with a circular core. The experiment consists of recording the transmission spectrum of another 25 cm-long piece of fiber for which a 5 μm lateral offset is applied with the injection fiber. As illustrated by Fig. 8, this situation, when compared to a centered injection [see Fig. 2(a) for L_{fiber} = 36 cm], puts in evidence several asymmetric peaks that appear for well-defined wavelength positions.

By applying the same procedure to the different silicon-core fibers that have been manufactured (not shown here), it has been validated that the peak positions depend on the core dimension and are poorly bend-sensitive. In the case of a fiber with silicon-core about 3 μm, the transmission spectrum has been recorded together with the intensity profile at the fiber output for different spectral positions. It is observed that the intensity profile is strongly modified at the peak wavelength—light is delocalized from the core—suggesting that these peaks are the signature of the cutoff wavelengths of the higher order core guided modes. It can be noted that the asymmetric shape of the peaks (front edge with steep slope at long wavelength and tail at short wavelength) is in accordance with the classical shape of cutoff peaks for which the mode is getting more and more confined in the core with the decrease in the wavelength (see Ref. 20). In the case of the silicon-core fiber, the higher-order mode that reaches its cutoff condition will be delocalized from the silicon core—i.e., be
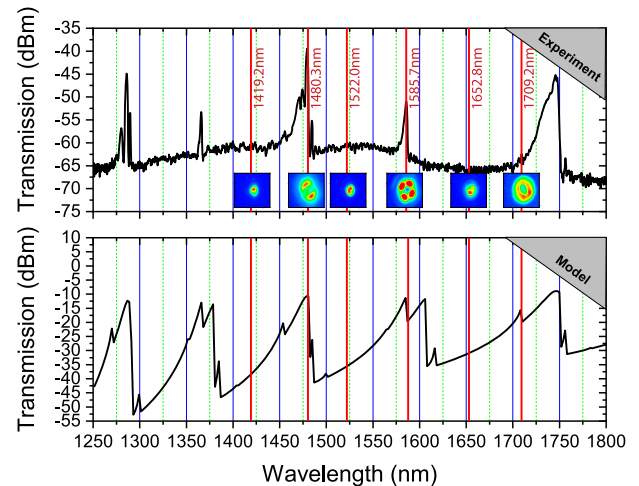
mostly located in the silica cladding—and hence experience better injection: better overlap integral with the offset excitation beam and lower Fresnel reflection. This assumption is confirmed by the calculation of the transmission of a piece of step-index 2.9 μm core diameter silicon fiber with a circular core and a homogeneous refractive index, submitted to the excitation of the mode of the high numerical aperture fiber used on our setup—whose wavelength dependence has been considered in the model—offset by 5 μm. As shown in Fig. 8, the calculated peak positions are in very good agreement with the observed ones. This is an additional proof that the optical behavior reported in this work is the one of a step-index silicon core fiber.

IV. CONCLUSION

In summary, it has been shown that the adoption of a two-step fiber manufacturing process is well suited to synthesize hundreds of meters-long silicon fibers with a small core dimension. The structural characterizations carried out on a piece of fiber obtained from this fiber drawing method converge toward the conclusion that a micrometer-size core can be obtained without any evidence of oxidation and with a well-organized crystalline structure disturbed only by the presence of a twin boundary along a core diameter. These structural elements are corroborated by the optical properties measured on several pieces of fibers, which, by analyzing the modal content, confirm the light guidance in a circular silicon core. All these properties are combined with low optical losses, which are thus obtained without requiring a specific preparation of the silicon material or post-treatment of the fiber. Such a post-treatment and especially the tapering of the fiber may likely be needed for nonlinear experiments so as to properly adjust the core dimension and, hence, the position of the zero-dispersion wavelength. It could also be helpful to further improve single crystallinity along the fiber. It has to be pointed out that the manufacturing technique disclosed here can been extended to the fabrication of more exotic geometries of fibers,

such as the PCFs. This underlines the potentiality of the technique to obtain fibers more complex than "simple" core/cladding structures. The authors also consider that the technique, similar to what has been demonstrated by MCD, can also be applied to other core materials.[21] Such fibers are now available for applications in photonics such as nonlinear photonics in the mid-IR region, which is the current trend in the community of research on silicon-core fibers.[10,22]

AUTHOR'S CONTRIBUTIONS

L.B. and G.B. designed the research. M.K., R.B., M.M., N.N., B.C., S.P., L.B., and R.H. carried out experiments and analyzed the data. G.B., K.B., and A.C. developed and fabricated the fibers. O.V. designed the fibers and performed theoretical modeling. L.B. and M.K. wrote the manuscript. All the authors contributed to scientific discussion and reviewed the manuscript.

ACKNOWLEDGMENTS

APPENDIX: EXPERIMENTAL SECTION/METHODS

1. Rod-in-stack

Silicon-core fibers fabricated by the rod-in-stack technique are produced by inserting a commercially available polycrystalline silicon rod (2 mm in diameter and about 50 mm in length) at the center of a stack of silica capillaries themselves previously drawn from a Suprasil silica tube (Fig. 9). Once sleeved into a 25 mm outer diameter tube, this stack is drawn into a cane under vacuum conditions so as to partly collapse all the holes of the air/silica cladding region. The cane (about 4 mm in diameter) with a core dimension about 300 μm in diameter is then inserted into a second tube (outer diameter 16 mm) and then drawn into a polymer-coated fiber on a conventional drawing tower. The outer diameter of the fiber is monitored all along fiber drawing. The drawing parameters are recalled in Table I.

2. Optical characterization

The transmission and modal properties of the fiber are characterized using a supercontinuum light source injected into a high numerical aperture fiber (UHNA3 from Nufern) butt-coupled to the
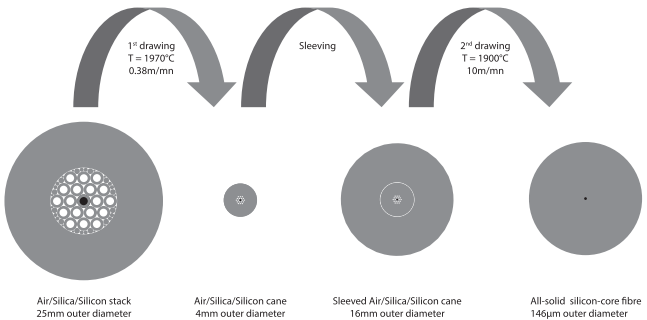

FIG. 9. Schematic of the rod-in-stack fabrication method and SEM image of the obtained fiber with a zoom on the core region.

silicon-core fiber under test. To record images of the modal content, the output of the silicon-core fiber is imaged on an InGaAs camera using a high numerical aperture micro-lens. So as to record the transmission properties of the fiber, the fiber output is butt-coupled to a multimode fiber connected to an Optical Spectrum Analyzer (OSA, Yokogawa 6370B), with the same injection procedure being applied. Background losses are obtained from the standard cutback procedure by cutting back the fiber from 146 cm to 36 cm in the case of Fig. 2. For all these characterizations, the fiber was coiled on bending radius about 5 cm in diameter and appeared to be poorly sensitive to bending. The same procedure has been applied to obtain the results of Fig. 8, except that the transmission spectrum has been obtained for an injection offset of 5 μm. The images have been recorded for the same offset injection together with the use of a tunable optical spectral filter after the supercontinuum source so as to capture images of a spectral bandwidth (about 1 nm) smaller than the peak FWHM.

3. Raman spectroscopy

Raman measurements were performed using an InVia Reflex Raman spectroscope (Renishaw). The spectral resolution was set to ~4 cm^{-1} with a holographic grating of 1800 grooves/mm and a Peltier cooled front illuminated CCD detector. The excitation radiation (λ = 514.5 nm) was produced by a DPSS laser (Cobolt®). An Olympus microscope was coupled to the spectrometer and Raman spectra were collected through a 100 × objective (0.9 N.A.) that provides a circular beam spot of 0.6 μm diameter. The laser power at sample was adjusted to 3 mW–4 mW, as measured by using

TABLE I. Drawing parameters.

Parameter	Value
Number of steps	2
Hot zone length	30 mm
Cane drawing (step 1)	Feed: 10 mm/mn typ. Draw: 0.3 m/mn typ.
Temperature (step 1)	1970 °C
Fiber drawing (step 2)	Feed: 1 mm/mn typ. Draw: 10 m/mn typ.
Temperature (step 2)	1900 °C

a Lasercheck power-meter (Coherent). High signal-to-noise-ratios (S/N) of individual spectra collected in this work were obtained with integration times of typically 2 s each. A fiber sample with a polished facet was used.

4. Scanning transmission electron microscopy (STEM)

Before characterization, fine samples have been prepared by extraction from a main sample consisting of a piece of fiber immersed into the resin. These thin slices, either transverse or longitudinal to the section of the fiber, are obtained by FIB (Focused Ion Beam). STEM images have been obtained using the FEI TITAN Themis 300 microscope. The TITAN Themis 300 S/TEM is equipped with a probe aberration corrector and monochromator, allowing a special resolution of 70 pm and an energy resolution of 100 meV. The microscope has also a super-X windowless four quadrant SDD (silicon drift detector) detection system for the STEM-EDX mapping and several annual dark field detectors. The experiment has been performed at 300 kV with a probe size of 500 pm, semi-convergence angle of 21 mrad, and a probe current of ~100 pA. For the high angle annular dark field (HAADF) images, collection angles have been between 50 mrad and 200 mrad.

5. Time of flight secondary ion mass spectrometry (ToF-SIMS)

As is the case for STEM, fine samples have first been prepared by FIB. ToF-SIMS analyses were carried out in order to obtain 3D chemical images of the optical fiber. A TOF.SIMS5 (ION-TOF Gmbh Germany) equipped with bismuth for primary ions and Cs+ for sputtering has been used. The fibers were analyzed with Bi^{3+} in burst alignment mode (a lateral resolution of 200 nm) over an area of $30 \times 30 \ \mu m^2$ with $128 \times 128 \ pixel^2$ in negative polarity. The depth profile was performed in non-interlaced mode with Cs^+ at 1 kV and 85 nA, rastered over $300 \times 300 \ \mu m^2$. After more than 30 000 s sputtering (15 000 scans), it was possible to reconstruct 3D images of the fiber.

DATA AVAILABILITY

The data that support the findings of this study are available from the corresponding author upon reasonable request.

REFERENCES

[1] M. A. Schmidt, M. Argyros, and F. Sorin, Adv. Opt. Mater. **4**, 13 (2016).

[2] P. J. A. Sazio, A. Amezcua-Correa, C. E. Finlayson, J. R. Hayes, T. J. Scheidemantel, N. F. Baril, B. R. Jackson, D.-J. Won, F. Zhang, E. R. Margine, V. Gopalan, V. H. Crespi, and J. Badding, Science **311**, 1583 (2006).

[3] J. Ballato, T. Hawkins, P. Foy, R. Stolen, B. Kokuoz, M. Ellison, C. McMillen, J. Reppert, A. M. Rao, M. Daw, S. Sharma, R. Shori, O. Stafsudd, R. R. Rice, and D. R. Powers, Opt. Express **16**, 18675 (2008).

[4] L. Lagonigro, N. Healy, J. R. Sparks, N. F. Baril, P. J. A. Sazio, J. V. Badding, and A. C. Peacock, "Low loss silicon fibers for photonics applications," Appl. Phys. Lett. **96**, 041105 (2010).

[5] N. Healy, U. Gibson, and A. C. Peacock, Semicond. Sci. Technol. **33**, 023001 (2018).

[6] A. C. Peacock, U. J. Gibson, and J. Ballato, Adv. Phys.: X **1**, 114 (2016).

[7] S. Morris, T. Hawkins, P. Foy, J. Hudson, L. Zhu, R. Stolen, R. Rice, and J. Ballato, Opt. Mater. Express **2**, 1511 (2012).

[8] N. Healy, M. Fokine, Y. Franz, T. Hawkins, M. Jones, J. Ballato, A. C. Peacock, and U. J. Gibson, Adv. Opt. Mater. **4**, 1004 (2016).

[9] X. Ji, S. Lei, S.-Y. Yu, H. Y. Cheng, W. Liu, N. Poilvert, Y. Xiong, I. Dabo, S. E. Mohney, J. V. Badding, and V. Gopalan, ACS Photonics **4**, 85 (2017).

[10] H. Ren, L. Shen, A. F. J. Runge, T. W. Hawkins, J. Ballato, U. Gibson, and A. C. Peacock, Light Sci. Appl. **8**, 105 (2019).

[11] A. C. Peacock and J. Ballato, "In-fiber silicon photonics," Opt. Photonics News **30**, 34–41 (2019).

[12] J. Ballato, T. Hawkins, P. Foy, B. Yazgan-Kokuoz, R. Stolen, C. McMillen, N. K. Hon, B. Jalali, and R. Rice, Opt. Express **17**, 8029 (2009).

[13] H. E. Hamzaoui, G. Bouwmans, B. Capoen, N. Chen, M. Douay, and M. Bouazaoui, Mater. Today Commun. **11**, 179 (2017).

[14] A. R. Zanatta, Sci. Rep. **9**, 11225 (2019).

[15] E. F. Nordstrand, A. N. Dibbs, A. J. Eraker, and U. J. Gibson, Opt. Mater. Express **3**, 651 (2013).

[16] A. Gumennik, L. Wei, G. Lestoquoy, A. M. Stolyarov, X. Jia, P. H. Rekemeyer, M. J. Smith, X. Liang, B. J. B. Grena, S. G. Johnson, S. Gradečak, A. F. Abouraddy, J. D. Joannopoulos, and Y. Fink, Nat. Commun. **4**, 2216 (2013).

[17] S. Chaudhuri, J. R. Sparks, X. Ji, M. Krishnamurthi, L. Shen, N. Healy, A. C. Peacock, V. Gopalan, and J. V. Badding, "Crystalline silicon optical fibers with low optical loss," ACS Photonics **3**, 378–384 (2016).

[18] A. Stoffers, B. Ziebarth, J. Barthel, O. Cojocaru-Mirédin, C. Elsässer, and D. Raabe, Phys. Rev. Lett. **115**, 235502 (2013).

[19] K. Chiba and S. Nakamura, Appl. Surf. Sci. **253**, 412 (2006).

[20] L. Jeunhomme, *Single-Mode Fiber Optics: Principles and Applications* (Dekker, 1990).

[21] S. Morris and J. Ballato, Am. Ceram. Soc. Bull. **92**, 24 (2013).

[22] H. Ren, L. Shen, D. Wu, O. Aktas, T. Hawkins, J. Ballato, U. J. Gibson, and A. C. Peacock, Opt. Mater. Express **9**, 1271 (2019).